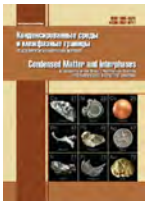

ISSN 1606-867X (Print)
ISSN 2687-0711 (Onine)
Condensed Matter and Interphases
Kondensirovannye Sredy i Mezhfaznye Granitsy
https://journals.vsu.ru/kcmf/

Original articles

Original article
https://doi.org/10.17308/kcmf.2021.23/3313

Synthesis, structure and superconducting properties of laminated thin film composites of $YBa_2Cu_3O_{7-\delta}/Y_2O_3$ as components of 2G HTS wires

A. E. Shchukin[1]✉, A. R. Kaul[1], A. L. Vasiliev[2, 3], I. A. Rudnev[4]

[1]Chemistry Department, Lomonosov Moscow State University, GSP-1, Leninskie Gory, Moscow 119991, Russian Federation

[2]National Research Center "Kurchatov Institute", 1 Akademika Kurchatova pl., Moscow 123182, Russian Federation

[3]Shubnikov Institute of Crystallography Russian Academy of Sciences 59 Leninsky pr., Moscow 119333, Russian Federation

[4]National Research Nuclear University "Moscow Engineering Physics Institute", 31 Kashirskoe shosse, Moscow 115409, Russian Federation

Abstract

2G HTS wires are capable of transferring huge amounts of electrical energy without loss. An increase in the current-carrying capacity in these materials is possible due to an increase in the thickness of the superconducting layer; however, there is a problem with the appearance of impurity orientations and other defects with increasing thickness. We have proposed a solution of this problem by increasing the thickness of the superconducting layer by the MOCVD method using interlayers of yttrium oxide.

The aim of this study was the production of thick composite films with yttrium oxide interlayers and high critical current density. In addition, we want to show the effectiveness of the approach of introducing yttrium oxide interlayers for the reduction of the number of parasitic orientations and defects with an increase in HTS film thickness.

The deposition of $YBa_2Cu_3O_{7-\delta}$ and Y_2O_3 films was carried out layer by layer using reel-to-reel MOCVD equipment. A 12 mm wire of the following architecture was used as a substrate: 200 nm $CeO_2(Gd_2O_3)$/30–50 nm $LaMnO_3$/5–7 nm IBAD-MgO/50 nm $LaMnO_3$/50 nm Al_2O_3/60 μm Hastelloy 276. The resulting films were annealed in oxygen for obtaining the orthorhombic YBCO phase.

$YBa_2Cu_3O_{7-\delta}/Y_2O_3$ composites were obtained. In these composites, obtained using the MOCVD method, the amount of side ($c_{\parallel}$) orientation of the HTS layer was reduced and high values of the critical current density, exceeding 1 MA/cm at a thickness of > 2 μm remained. The efficiency of the approach of introducing yttrium oxide interlayers for the increase in the current characteristics with increasing film thickness was shown. It was found that further thickening of films with interlayers is prevented by the formation of nanopores, reducing the critical current density.

Keywords: YBCO, MOCVD, Heterostructures, Buffer layers, Y_2O_3, HTS, Superconductor

Acknowledgements: the study was carried out within the framework of the RFMEFI 58214X0005 project with the support of the Ministry of Education and Science within the framework of event 1.4 "Applied research aimed at solving complex scientific and technological problems."

For citation: Shchukin A. E., Kaul A. R., Vasiliev A. L., Rudnev I. A. Synthesis, structure and superconducting properties of laminated thin film composites $YBa_2Cu_3O_{7-\delta}/Y_2O_3$ as the components of 2G HTS wires. *Kondensirovannye sredy i mezhfaznye granitsy = Condensed Matter and Interphases*. 2021;23(1): 122–139. https://doi.org/10.17308/kcmf.2021.23/3313

✉ Shchukin Alexander E., email: aleksandr.shukin@mail.ru

Для цитирования: Щукин А. Е., Кауль А. Р., Васильев А. Л., Руднев И. А. Синтез, структура и сверхпроводящие свойства тонкопленочных слоистых композитов $YBa_2Cu_3O_{7-\delta}/Y_2O_3$ как компонентов ВТСП-лент второго поколения. *Конденсированные среды и межфазные границы*. 2021;23(1): 122–139. https://doi.org/10.17308/kcmf.2021.23/3313

1. Introduction

The last 15 years in the field of applied superconductivity have been marked by the development of technology for the production of long wires, in which the current-carrying layer is a thin film of high-temperature superconductor $RBa_2Cu_3O_{7-x}$ (RBCO, R = REE, Y) grown epitaxially on oxide buffer layers covering the base metal wire. Such materials, called 2G HTS wires (2G coated conductors), have already proven their effectiveness in the electric power industry for the transmission of electricity through superconducting cables, for production of motors, generators, current limiters, transformers and other electrical equipment with record power and weight and size characteristics [1, 2]. The development of magnets for accelerators and fusion reactors, 10 MW wind turbines, superconducting energy storage devices, levitation bearings, high-resolution medical tomographs and many other fundamentally new devices for various fields of technology, from the extractive industries to aerospace industry is performed using 2G HTS wires [3–7]. The efficiency of superconducting materials directly depends on the critical current density characterizing them (*j*c). The high *j*c values, inherent to RBCO heteroepitaxial thin films, occur for two reasons: 1) their structure approaches a two-dimensional mosaic monocrystal with a small misorientation of neighbouring grains, which reduces the likelihood of the appearance of the so-called "weak links" characteristic for polycrystalline HTS ceramics and strongly limiting *j*c; 2) their structure contains a large number of nonequilibrium defects – misfit dislocations, packing defects, antistructural defects formed during film growth, and preventing magnetic vortex creep. However, along with the listed "useful" defects in RBCO films, morphological defects reducing the *j*c value are often formed. First of all, such defects include crystallites with the orientation of the CuO_2 planes perpendicular to the substrate plane. It is known [8, 9] that the crystal structure of the $RBa_2Cu_3O_{7-\delta}$ orthorhombic phases (Fig. 1a) is highly anisotropic, and the superconducting current in them propagates along the CuO_2, therefore, the achievement of the maximum *j*c values requires RBCO film growth in the <001> direction, e.g. along the *c* axis, perpendicular to the substrate plane ($c_\perp$ in Fig. 1b). The growth of RBCO films with other axial orientations (*a* and *b* oriented growth, hereinafter not distinguished by us and denoted as $c_\parallel$) not only significantly reduces the superconducting current [10], but also prevents a further increase in the thickness of the $c_\perp$ oriented film.

In many studies devoted to the formation and properties of superconducting epitaxial $c_\perp$ RBCO

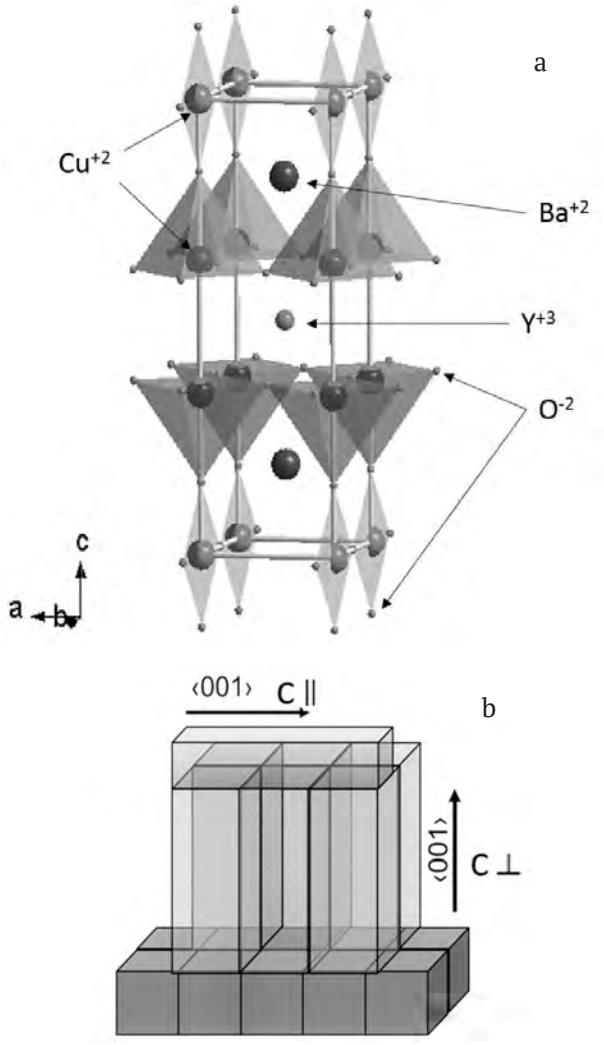

Fig. 1. Structure $YBa_2Cu_3O_{7-\delta}$ (a); Schematic picture of $c_\perp$ grains heteroepitaxy and further $c_\parallel$ RBCO grains growth (b)

films, the problem of obtaining high *jc* values in the upper layers of films with a thickness of about 1 μm was revealed [11, 12]. With increasing thickness, the oriented crystallization of the layers changes from the predominant $c_{\perp}$ to the preferential $c_{\parallel}$ (Fig.1b). This phenomenon does not allow an arbitrary increase in the value of the superconducting current by a proportional thickness increase of the RBCO layers. Discussing various physicochemical reasons for switching the growth direction, it is important to understand that the $c_{\perp}$ orientation is thermodynamically preferable (corresponds to the minimum energy of the heteroepitaxial system), and the appearance of the $c_{\parallel}$-orientation is caused by kinetic reasons. The deposition of the HTS layer is carried out by various methods, but in all cases it is performed on a substrate heated to 750–900 °C. Increasing the thickness of the HTS layer leads to a decrease in the actual temperature of the growth surface and slows down the mass transfer in the surface layer. Under these conditions (as well as at an insufficiently high temperature of film deposition and/or an excessively high rate of their deposition), the $c_{\parallel}$-orientation becomes advantageous, since the fastest growth occurs along *ab*-planes, which is typical for all layered crystals. The complete match of the unit cell (UC) parameters at the interface $c_{\parallel}/c_{\perp}$ (Fig. 1b) contributes to the nucleation of crystallites with a $c_{\parallel}$-orientation, i.e., crystallites oriented as $c_{\perp}$, prove to be an excellent substrate for the growth of $c_{\parallel}$-oriented crystallites. The critical nucleus of $c_{\parallel}$-oriented crystallites in this situation has a minimum size, and its formation is characterized by a minimum energy barrier [13].

According to the literature, for the suppression of grain growth in the $c_{\parallel}$-orientation it is recommended to change the deposition conditions of HTS layers as their thickness grows, namely: an increase in the deposition temperature, a decrease in oxygen pressure (which also increases the diffusion mobility in R-Ba-Cu-O systems) and/or a decrease in the deposition rate [14]. Another approach recommended in [13, 15], proposes the use of buffer layers with an increased mismatch of the UC parameters in HTS/buffer layer interface.

In this study, we proposed suppressing the growth of $c_{\parallel}$-crystallites by introducing intermediate Y_2O_3 layers of nanometer-scale thickness in YBCO matrix. Yttrium oxide forms heteroepitaxial boundaries with YBCO, since the difference between UC and YBCO parameters is small, its introduction should not prevent $c_{\perp}$ YBCO epitaxial growth. It was previously noted [16] that in thin YBCO films containing an excess of Y_2O_3, the density of $c_{\parallel}$-crystallites decreases. These features allowed us to assume that laminated two-phase composites YBCO/Y_2O_3 deposited to metal wires with biaxially textured buffer layers can be formed with a predominant $c_{\perp}$ orientation of crystallites to a higher thickness than layers of stoichiometric composition ($YBa_2Cu_3O_{7-\delta}$), and therefore, with equal thickness, they can have a higher critical current density.

The deposition of HTS layers was carried out on moving substrate wires used in the 2G HTS wire technology by metal-organic chemical vapour deposition (MOCVD). The peculiarity of this method is the transport of the film's metal components to the reactor in the form of vapours of metal-organic volatile compounds (precursors). In presence of oxygen these components decompose on a heated substrate with the formation of an oxide film. This method allows the formation of films, uniform in composition and thickness, on the substrates of complex shapes and large area, including the continuous sputtering of a film on a long metal wire in reel-to-reel mode. Today, MOCVD technology is one of the most popular in the production of 2G HTS wires, and wires obtained using this technology are not inferior in characteristics to wires formed by laser ablation [17].

This study presents the results of comparative studies of the texture, microstructure, and current-carrying properties of YBCO films and two-phase laminated YBCO/Y_2O_3 composites of various thicknesses.

2. Experimental

The deposition of films was carried out using reel-to-reel MOCVD equipment (Fig. 2). Solid mixtures of complex compounds of yttrium, barium, and copper with dipivaloylmethane were used as precursors: $Y(thd)_3$, $Ba(thd)_2$(tetraglyme), $Cu(thd)_2$. Since the long-term exposure of the precursors at high temperatures leads to the gradual loss of their ability to sublimation, the sublimation was carried out by the flash

evaporation of micro-portions of the solid mixture of the listed precursors. For this, a tablet (*1*) obtained by pressing previously purified by sublimation (in the case of $Ba(thd)_2$(tetraglyme) - recrystallization) and thoroughly mixed precursors, was placed in an automatic dispenser, which includes a device for microstepping the tablet and a knife moving reciprocally in the direction transverse to the axis of tablet movement. With the simultaneous movement of the tablet and the knife, very thin layers of the precursor mixture were cut off, which turned into a continuous stream of fine particles. Then these particles, entrained by the argon flow, entered the evaporator (2), heated to 335 °C, where they were instantly evaporated. From the evaporator, the flow of Ar and precursor vapours were directed along a metal tube heated to 320 °C (*3*) into the hot (T = 350 °C) distributor unit (*4*), in which it was mixed with an oxygen flow and divided into 8 equal parts, uniformly distributed along the entire length of the deposition zone (5). On both sides of the precursor vapour outlet openings into the deposition zone, there were outlets for additional argon flow, which forms gas "curtains" (*8*), directing the precursor vapours onto the substrate wire which is heated to 820–850 °C. A reel with the rewind ability (*7*), driven by a stepper motor, allowed setting the required rewind speed (up to 30 mm/s), and a braking asynchronous motor on the feed reel allowed to keep the wire tension necessary for reliable thermal contact of the wire with the heated "table". When the precursors vapours with oxygen reached the heated substrate wire, oxidative thermolysis occurred with the formation of an oxide film on the substrate surface. The gas products of this reaction, together with the unreacted vapours of the precursors, were pumped out by a pump supplied with dust filter. The pressure of 3.5 mbar was maintained in the reactor by a control valve at the outlet of the reactor. All gas flows were controlled by gas flow regulators. For the deposition of the HTS film, an extensive preliminary study on the selection of the optimal gas flows and temperatures for each of the heating zones of the MOCVD unit was performed.

As substrates, metal wires made of the heat-resistant Hastelloy 276 alloy, covered with buffer layers with the following multilayer architecture: 200 nm $CeO_2(Gd_2O_3)$/30–50 nm $LaMnO_3$/5–7 nm IBAD-MgO/50 nm $LaMnO_3$/50 nm Al_2O_3/60 μm Hastelloy were used. The amorphous Al_2O_3 layer prevented the oxidation of the metal wire and

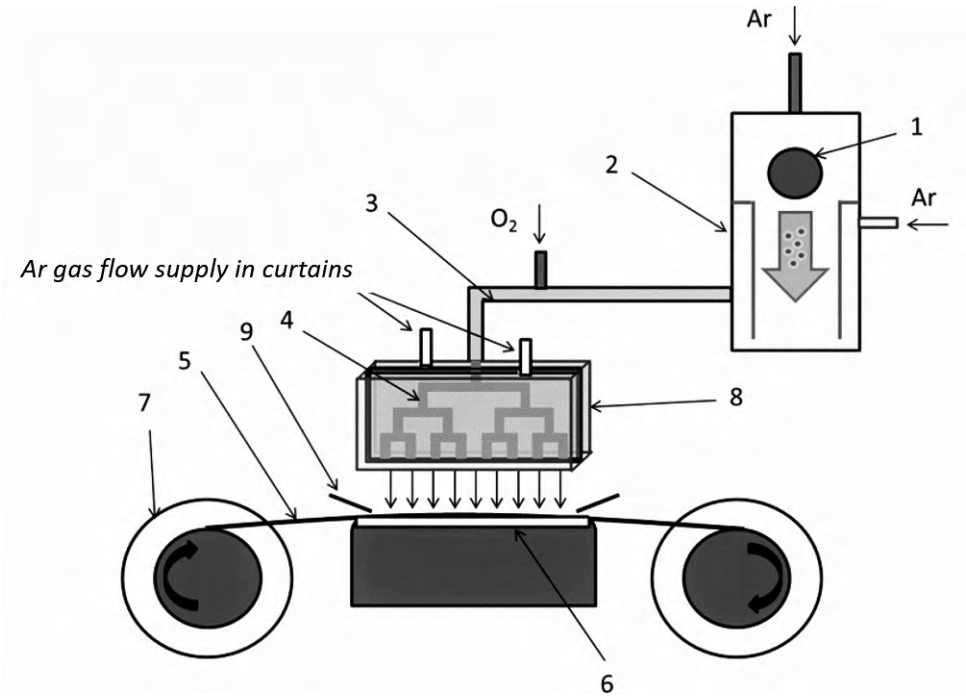

Fig. 2. MOCVD equipment scheme: Precursor tablet (*1*), Evaporator (*2*), Transportation pipe (*3*), Distributor (*4*), Wire (*5*), "Table" (*6*) with heating, Reel with rewinding (*7*), "Curtains" (*8*), Windscreens (*9*), that restrict precursor deposition on unheated wire parts

the diffusion of its components into the HTS layer during its high-temperature deposition; the next $LaMnO_3$ layer reduced the roughness of the growth surface and prevented the interaction of the Al_2O_3 and MgO layers. The biaxial texture was created in MgO layer applied over $LaMnO_3$ by ion beam assisted deposition (IBAD). The biaxial texture was transferred epitaxially to the deposited $LaMnO_3$ layer and then to the final buffer layer of $CeO_2(Gd_2O_3)$ solid solution, which has a slight mismatch between the UC and YBCO parameters, also contributing to a decrease in the number of $c_{\parallel}$-oriented crystallites in the film [18–21]. All used substrates were 12 mm wide; therefore, the absolute values of the critical current given below refer to this width of the superconducting layer.

It is known that the MOCVD process of multicomponent compounds is incongruent, since the precursors of different metals have differing values of volatility and thermal stability. Therefore, the deposition process of superconducting layers was preceded by the stage of optimization of the precursors ratio in the initial mixture of precursors. The elemental composition of the obtained films, their phase composition and the superconducting critical current were studied. Thus, the region of optimal composition of the films and the molar ratio of precursors 1(Y):1.18(Ba):1.56(Cu) were established for the optimal T-pO_2 deposition conditions.

When choosing these conditions, we were guided by the diagram described in [22], while taking into account the features of the MOCVD technology used (reel-to-reel unit, the use of a "table" as a heating element): the temperature of the heating element was 990 °C, the reel-to-reel speed was 2 mm/s, the precursor feed rate was 9.6 g/h. In all experiments, an oxygen partial pressure of 1.6 mbar was maintained; constancy of pO_2 is extremely important, since this parameter has the greatest effect on the elemental ratio in the deposited films. For samples with intermediate Y_2O_3 layers the deposition of the latter was carried out at a temperature of 800 °C, wire reeling speed was 10 mm/s and $Y(thd)_3$ precursor feed rate was 3.2 g/h.

During high-temperature film deposition, the YBCO phase was formed in the non-superconducting tetragonal modification with the composition $YBa_2Cu_3O_{6.5}$. For the transfer of YBCO into the superconducting orthorhombic phase, the obtained samples were oxidized in an oven at 450 °C and atmospheric pressure with an additional supply of oxygen and subsequent slow cooling.

2.1. Study of the elemental and phase compositions of films, their morphology; method for the determination of $c_{\parallel}$-oriented grains concentration

Determination of the phase composition of the films was carried out using Rigaku D/MAX 2500 and Rigaku SmartLab diffractometers with a Ge (220)×2 monochromator with a primary beam using Cu-K_α radiation (λ = 1.54046 Å). Diffraction patterns were recorded with Bragg–Brentano geometry (Siemens, Rigaku D /MAX) or with a parallel beam (Rigaku SmartLab). Scanning was performed in the θ-2θ scan mode with 0.02° steps. The surface morphology of the films was investigated using scanning electron microscopy (SEM) with JEOL and LEO Supra 50 VP (LEO, Germany) with a magnification up to 200000.

Cross-sectioned samples were prepared using a Ga^+ focused ion beam (FIB)$^+$ and HeliosNanoLab™ 600i (FEI, USA) electron-ion microscope for investigation by transmission and scanning transmission electron microscopy (TEM and STEM, respectively). For the prevention of damage to the sample surface, a protective platinum layer with a thickness of about 1.5 μm was deposited on the film surface before starting the standard procedure for preparing a cross section by the FIB method. Then the thin sample was cut out using focused ion beam with Ga^+ energy E = 30 keV and current I = 6.5 nA. This sample was transferred using an Omniprobe 200 manipulator (Omniprobe, USA) directly in the microscope chamber and welded by the deposition of tungsten onto a special copper grid. During the last stage, the sample was successively thinned using FIB while changing the ion beam parameters to E = 2 keV, I = 28 pA.

The studies were carried out using TITAN 80-300 TEM/STEM (FEI, USA) with an accelerating voltage of 300 kV, equipped with a spherical aberration corrector, high-angle annular dark-field detector (HAADF) (Fischione, USA), an

analyser of characteristic electron energy losses (GIF, Gatan, USA) and an energy-dispersive X-ray spectrometer (EDAX, USA).

Since $c_{\parallel}$-oriented YBCO grains are formed predominantly in the upper part of the superconducting layer; the method of X-ray phase analysis turned out to be insufficiently informative for their quantitative determination and even can provide incorrect information about their content on the surface. Thus, it was important to develop a quantitative detection method of $c_{\parallel}$-grains on the surface of the YBCO film. For the determination of surface concentration of $c_{\parallel}$-oriented crystallites, the SEM data were processed using the ImageJ software, which allowed distinguishing zones with different brightness of grey after transforming the original image into an image with a combination of two contrasting colours (Fig. 3).

In Fig. 3a $c_{\parallel}$-oriented grains which on SEM images look like bright and light stripes can be clearly seen against the background of $c_{\perp}$ matrix. Areas occupied by $c_{\parallel}$-oriented crystallites can be selected and determination of the fraction of the surface area occupied by these crystallites can be performed using the ImageJ program (Fig. 3b).

2.2. Critical current measurement by the "Superscan" method

Two methods for the determination of critical current were used in the study: contactless Superscan technique and four probe method for measuring current-voltage characteristics. The latter was also used for the calibration of the Superscan technique, which is described below. The Superscan method was implemented using a unit, the design and the measurement principle of which are shown in Fig. 4a. During the measurement of the critical current, the wire was rewound from reel to reel, passing through a Dewar vessel with liquid nitrogen, where it cooled and transferred into a superconducting state, passed between two poles of a permanent magnet (0.15 T) and then passed through a head with 9 Hall sensors covering the entire width of the wire. Since YBCO is a type II superconductor, the magnetic field penetrates into the superconducting layer and initiates an eddy current along the length of the wire. Hall sensors measured the value of magnetic induction corresponding to the current in the wire. The signals from the Hall sensors were recorded in a file containing all information about the distribution of current along the width and length of the wire, the file was analysed using a computer program. The final presentation of the results allowed determining the current distribution of the critical current along the width (transverse component) and the length of the wire (longitudinal component) (Fig. 4a). In most cases, the values of the critical current obtained in this way were in good agreement with the

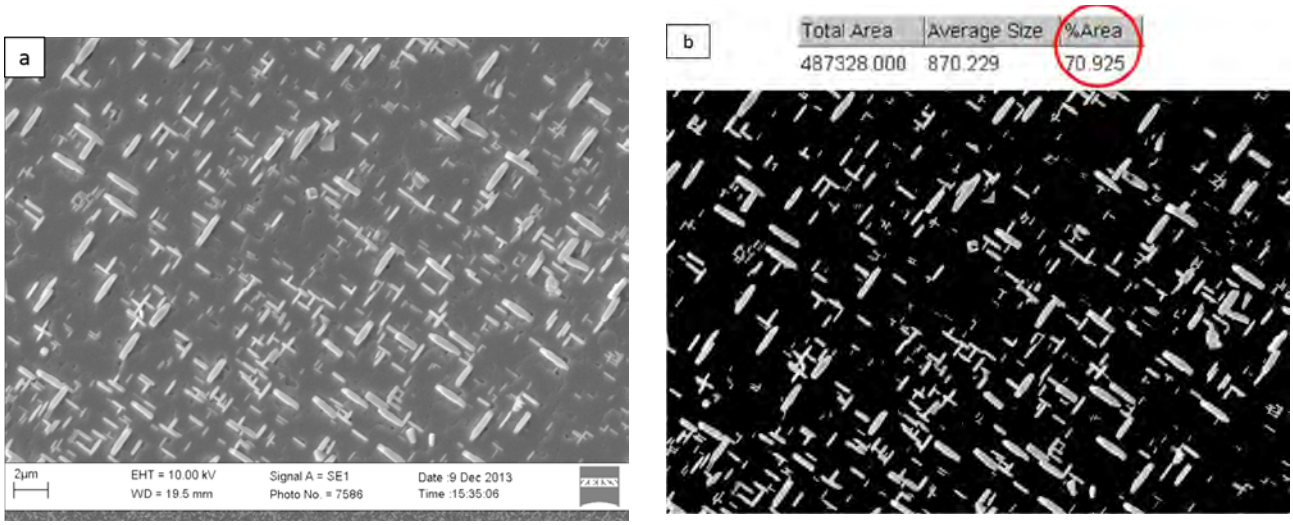

Fig. 3. Calculations of $c_{\parallel}$-oriented grains using the ImageJ Software: SEM image (up view) of the YBCO film surface (a), SEM image processing with the same area: $c_{\parallel}$-oriented grains are white coloured, $c_{\perp}$ grains are black (b)

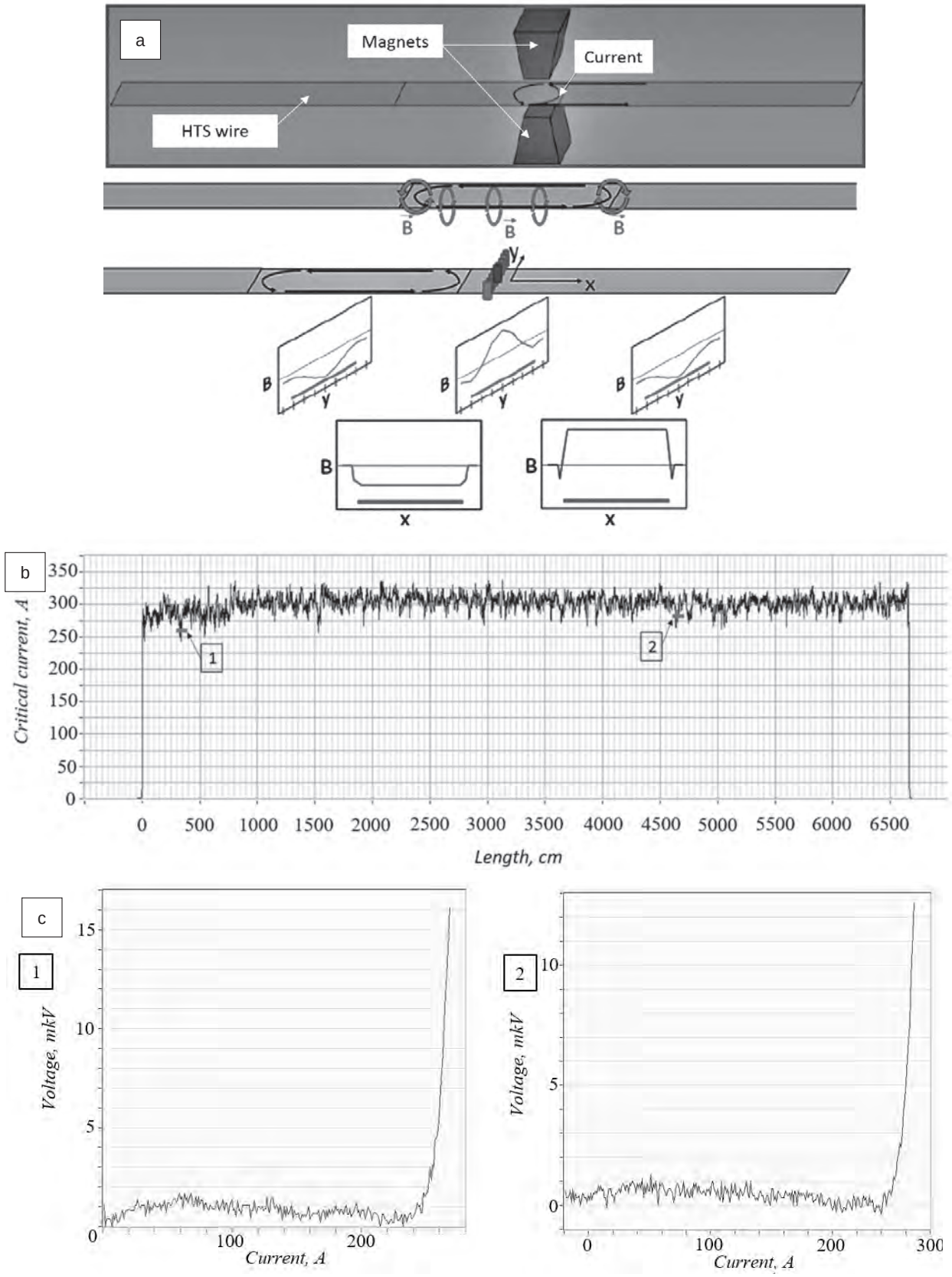

Fig. 4. SuperSCAN method: Operating principle and obtained information (a), the comparison of SuperSCAN method measurements (b) with 4-point probe measurements of segments 300–400 cm (1) and 4600–4700 cm (2) (c)

results of direct measurements of the current-voltage characteristics obtained by the four probe method, as it can be seen from Fig.4(b and c). The data for 1 m long sample are shown; it proves the reliability of the Superscan technique.

3. Results and discussion

Numerous studies of the structure and properties of epitaxial films of RBaCuO superconductors indicated that *jc* values of films strongly depend on the cationic R:Ba:Cu ratio with the best *jc* values achieved not in single-phase films with a stoichiometric cation ratio of 1:2:3, but in those with a significant deviation from this composition. Since the $YBa_2Cu_3O_{7-x}$ phase does not have a homogeneity range for cations, impurity phases appear with a deviation from the ratio of 1:2:3. The resulting phase ensembles containing the dominant epitaxial phase of $YBa_2Cu_3O_{7-x}$ differ from equilibrium phase ensembles with the same ratio of elements in polycrystalline powder compositions or polycrystalline films. Thus, in the presence of an excess of barium and copper oxides in equilibrium polycrystalline samples, the $BaCuO_2$ phase coexists with the $YBa_2Cu_3O_{7-x}$ phase [23–25]. However, this impurity phase was not observed in epitaxial films of (001) $RBa_2Cu_3O_7$ (R = Lu, Ho, Y, Gd, Nd). In this case, instead of it, (001)-oriented Ba_2CuO_3 and $BaCu_3O_4$ phases were formed, and the latter existed only until epitaxial contact with the $YBa_2Cu_3O_{7-x}$. A similar phenomenon was observed with an excess of yttrium: the non-superconducting Y_2BaCuO_5 phase was thermodynamically stable in polycrystalline samples. However, in thin films with an excess of yttrium in the matrix of the $YBa_2Cu_3O_{7-x}$ epitaxial film, Y_2O_3 nanoinclusions with the size of 3–20 nm appeared [25]. These and similar phenomena were interpreted as a manifestation of epitaxial phase stabilization due to the low energy of epitaxial interfaces [26].

Ba_2CuO_3 and $BaCu_3O_4$ phases formed with an excess of barium and copper had a negative effect on the superconducting properties of the epitaxial HTS film, while Y_2O_3 nanoinclusions on the contrary improved them, being additional pinning centres for the magnetic vortices, increasing the stability of the critical current of the HTS film in strong magnetic fields. Moreover, the excess of Y_2O_3 in the film shifted the phase ensemble to the YBCO–Y_2O_3–CuO_x region with a lower melting point, which accelerated diffusion and suppressed the growth of ***a***-oriented crystallites, and this, in turn, led to a significant increase in the critical current density [16]. The foregoing considerations explain why, during the deposition of YBCO films, we deliberately made an effort to obtain compositions with an excess of yttrium, composing the corresponding mixtures of volatile precursors and considering the incongruence of the MOCVD process. As a result of a large number of iterative experiments, we found the optimal ratio of precursors 1(Y):1.18(Ba):1.56(Cu), which provided the highest critical current under the chosen deposition conditions (at 77 K, H = 0) for films of the same thickness.

In the XRD spectra of heteroepitaxial YBCO layers with an excess of yttrium (Fig. 5), Y_2O_3 impurity in the form of dispersed particles oriented by the <110> axis perpendicular to the *ab*-planes of the matrix of the $YBa_2Cu_3O_{7-x}$ phase, as evidenced by a blurred reflex (440) was observed. In the context of the present study, the ratio between the (006) and (200) reflections of the $YBa_2Cu_3O_{7-x}$ phase corresponding to $c_\perp$ and $c_\parallel$-crystallites, respectively, was of interest. Cuttings of the XRD spectra, including these reflections for four film samples of different thicknesses are shown in Fig. 5. The volume content of the $c_\parallel$-phase (VC) can be determined through the area ratio of the (200) and (006) peaks, found by plotting curves, approximating each peak separately: VC of $c_\parallel$-phase = $S_\parallel / (S_\perp + S_\parallel)$. VC values of $c_\parallel$-phases calculated from the spectra presented in Fig. 5 were 0%, 2.4%, 7.4%, and 63.7% for samples 1–4, respectively.

The above procedure for determining the surface content of the $c_\parallel$-phase according to SEM data allowed establishing the fraction of the film surface occupied by $c_\parallel$-crystallites for the same samples. Microphotographs of the surface of the films of samples 1-4 are shown in Fig. 6.

These results (Figs. 5 and 6), as well as a quantitative comparison of the XRD and SEM results for films of successively increasing thickness (Fig. 7) allowed us to conclude that $c_\parallel$-crystallites were located mainly on the surface of the films and, as the thickness of the film increased, gradually filled its surface completely. The dependence in Fig. 7 shows a clear non-

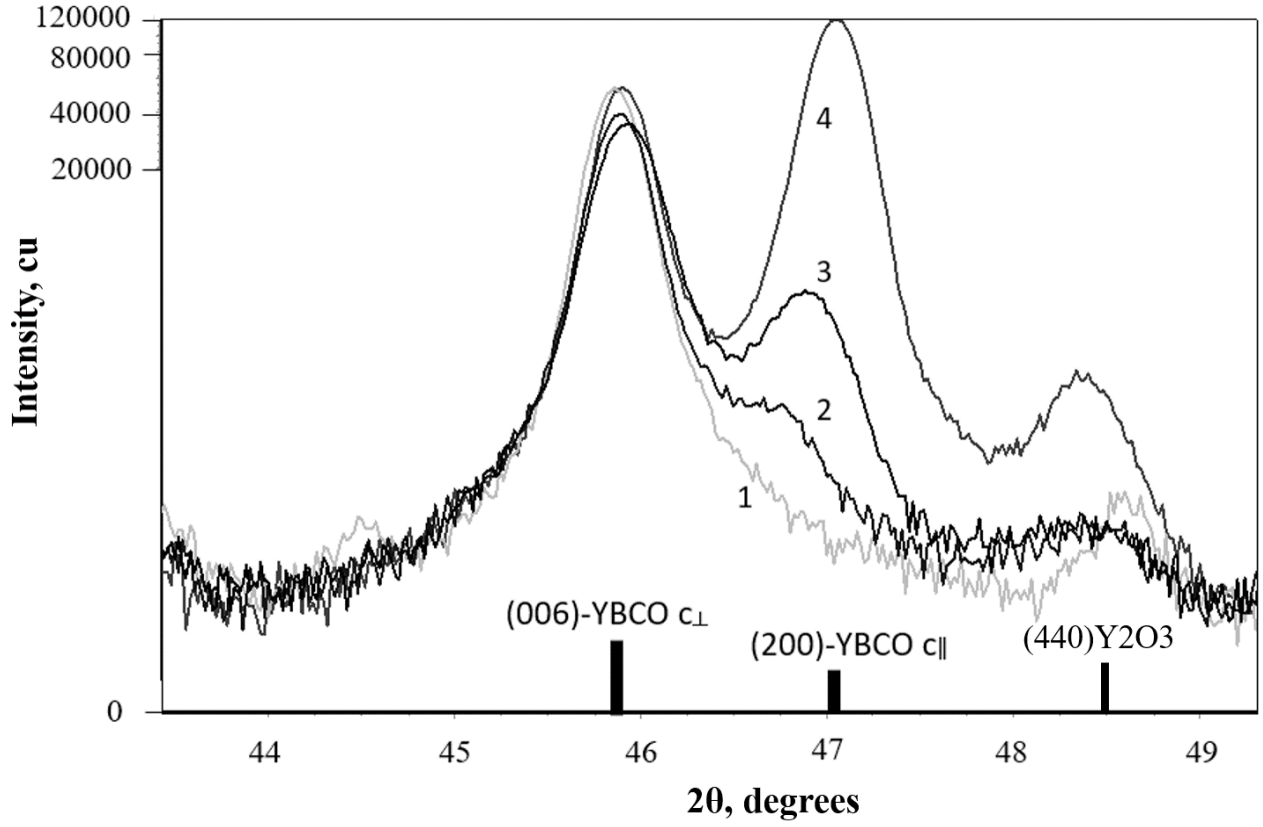

Fig. 5. XRD graphs for the samples 1–4 with different quantities of $c_{\parallel}$-oriented grains

linear course corresponding to our ideas about the development of growth of $c_{\parallel}$-crystallites in the following stages:

1. The formation of nuclei – at this stage, the competitive nucleation of crystallites of the $YBa_2Cu_3O_{6,5}$ phase in $c_{\perp}$ and $c_{\parallel}$-orientations and their initial growth occurred.

2. Extensive growth of nucleated crystallites of the $c_{\parallel}$-phases on the surface of the film, as well as the formation of new nuclei of this orientation. The development of the process at this stage is facilitated by three features: a) lamellar crystallites of the tetragonal phase grow faster along the base plane *ab,* than in the perpendicular direction (single crystals of $YBa_2Cu_3O_{6.5}$ phase look as thin plates), b) $c_{\parallel}$-crystallites protrude above the growth surface and therefore were the first to meet the flow of the material feeding the film during the growth of the HTS layer from the gas phase, c) $c_{\parallel}$-oriented crystallites were easily formed on $c_{\perp}$ oriented crystallites, while the opposite was not observed.

3. Full surface coverage with $c_{\parallel}$-crystallites, while there was practically no growth of $c_{\perp}$ phases. The combined action of the factors listed in the description of stage 2, as the film thickness increased, led to the growth of colonies of $c_{\parallel}$-oriented crystallites, which, as a result, covered the entire surface of the film, suppressing the growth of a conductive $c_{\perp}$ oriented layer.

The results shown in Fig. 7, clearly demonstrated that surface analysis was the most important stage in the study of the growth of YBCO films (more indicative than XRD), since it allowed understanding whether there is a possibility of increasing the critical current with increasing film thickness. Thus, if, according to XRD data, the volume content of the $c_{\parallel}$- phase in the film was still not high and it was at the level of 20-30%, then the surface may already be so filled with this phase that further deposition of HTS layers became ineffective in terms of increasing the critical current. This is illustrated in Fig. 8, showing the results of measurements of critical currents (I_c) and the microstructure of the surface of the HTS layer, which was grown in thickness (h) in 6 consecutive cycles of the YBCO deposition. It can be seen that at a thickness (h)

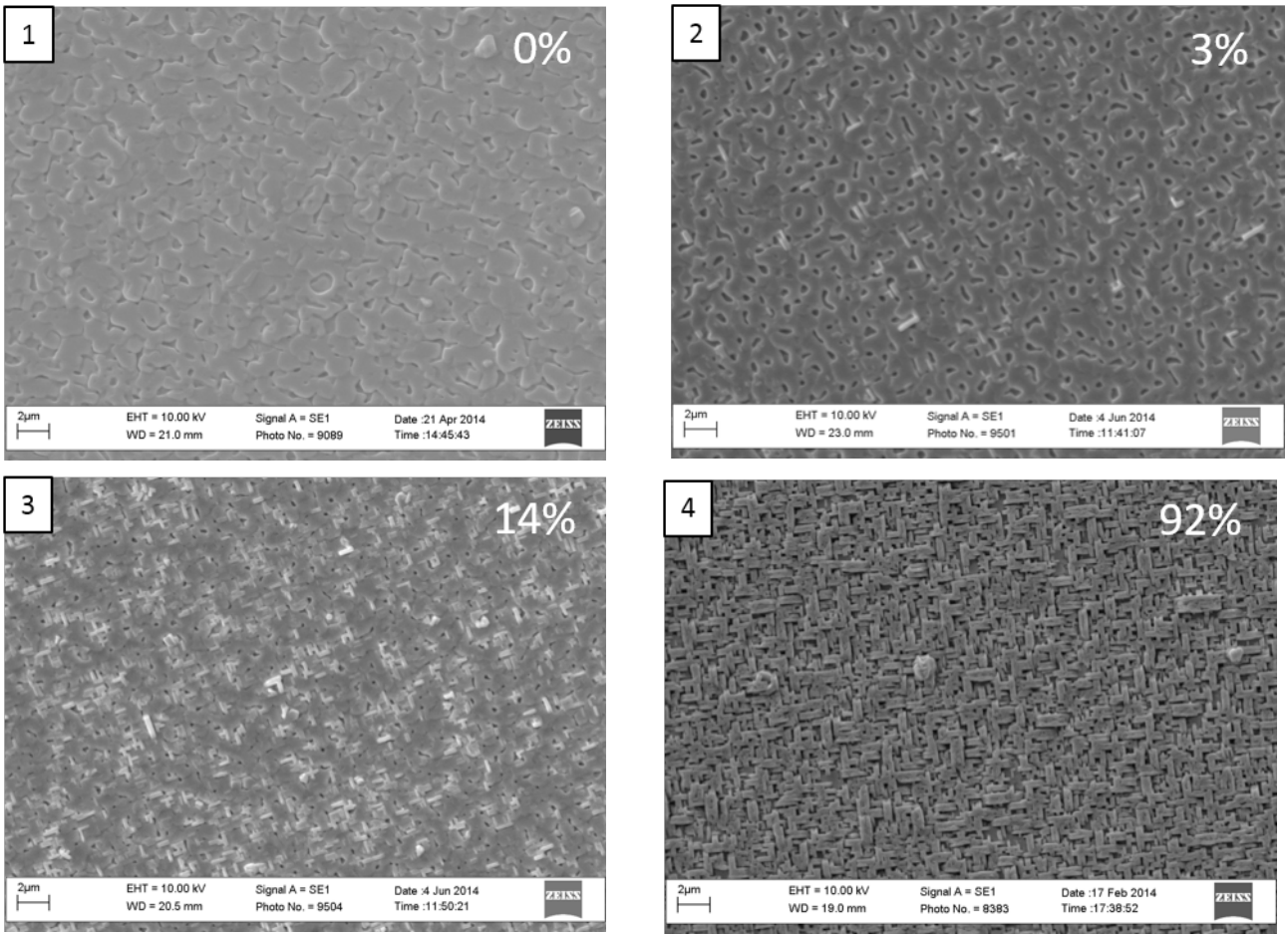

Fig. 6. SEM images of 1-4 samples. The calculated content of $c_{\parallel}$-oriented grains on the film surface is indicated on the corresponding photo

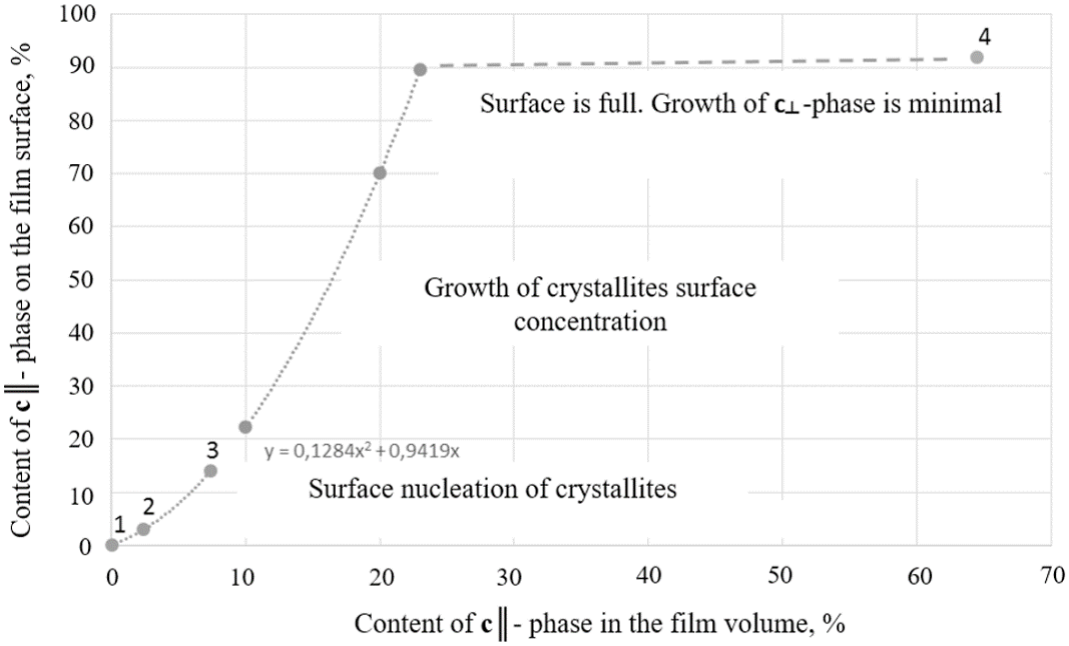

Fig. 7. The dependence between the volume content of the $c_{\parallel}$-oriented phase (from XRD data) and the surface content of crystallites with this orientation (from the SEM data) on the $YBa_2Cu_3O_{7-\delta}$ film surface with increasing thickness (thickness increasing along the X-axis)

of about 1900 nm, the slope of the dependence I_c (h) changed sharply, and with further thickening of the HTS layer, its critical current increased insignificantly (Fig.8a), which was a direct consequence of the fact that at a thickness of 1900 nm the film surface was almost completely blocked with $c_{\parallel}$-oriented crystallites (Fig. 8d).

It was already noted above that the change in growth from a thermodynamically stable $c_{\perp}$ orientation to a kinetically favourable $c_{\parallel}$-orientation was promoted by lowering the temperature of the film growth surface. In this context it is important to understand the reasons for this cooling. Assuming that the total thermal effect of decomposition and oxidation of volatile precursors of metal components of YBCO in the MOCVD process is low, it can be argued that the temperature of the growth surface reflects the ratio of the heat flux coming from the heater located under the substrate to the radiant energy flux emitted by the heated wire surface. The dependence of the thermal conductivity of the YBCO film on its thickness in the direction perpendicular to the substrate is difficult to predict *a priori,* since it is influenced by many factors. The crystalline anisotropy of the superconducting phase causes the anisotropy of thermal conductivity: in the direction of the *c* axis (i.e. perpendicular to the substrate) the thermal conductivity was 4–10 times lower than along the substrate [27]. The uncertainty in the value of the anisotropy factor was associated with the dependence of the phonon thermal conductivity (it dominates at a high temperature of film deposition) on the crystallite size of the film, which depended on the method and conditions of film deposition, but increases with increasing film thickness. At the same time, the fraction of $c_{\parallel}$-crystallites increased, which, as well as the coarsening of grains, contributed

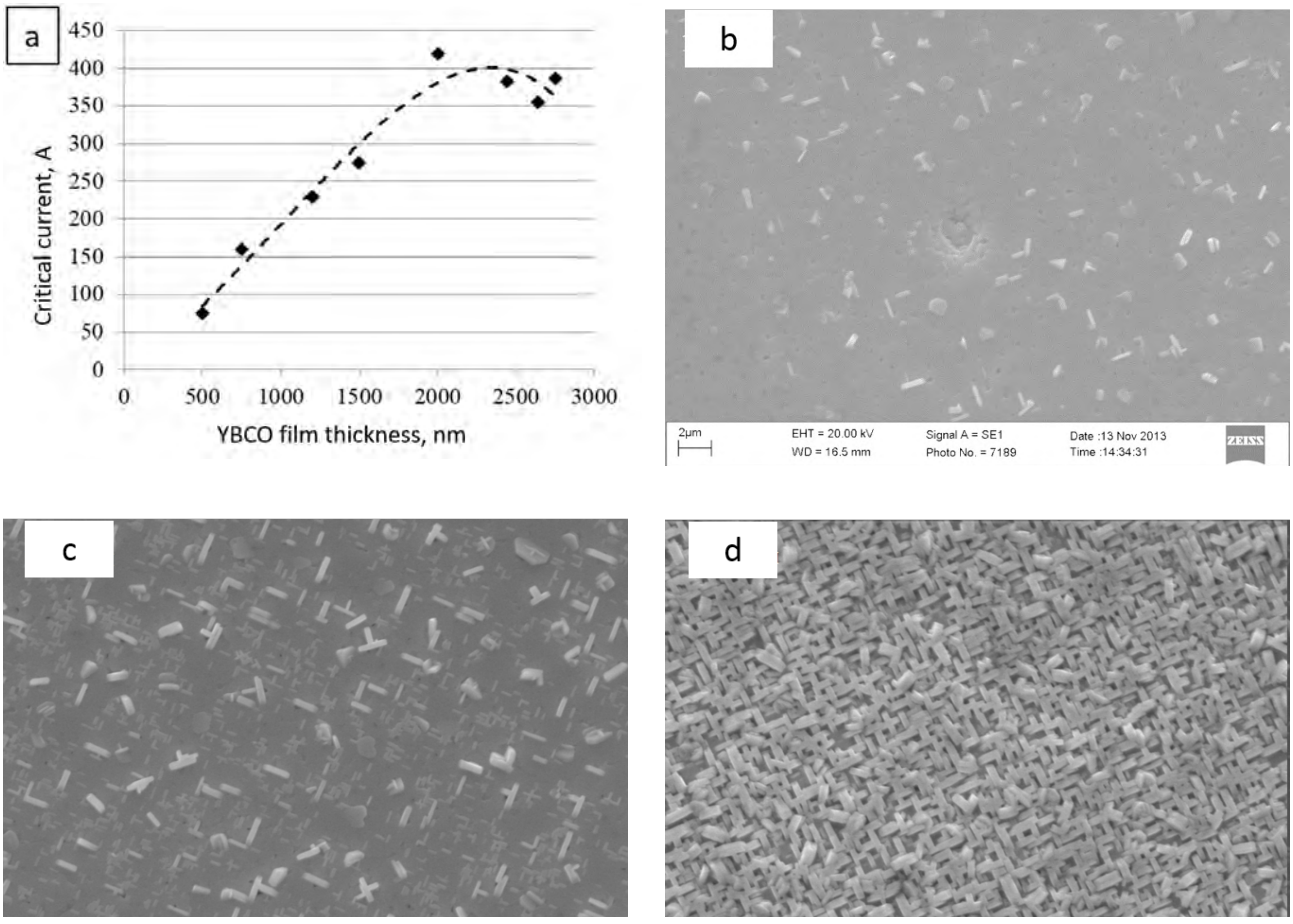

Fig. 8. a) The thickness dependence of critical current in YBCO films produced in 6 sequential MOCVD cycles; b–d – the YBCO film surface evolution with an increase in its thickness (thickness is shown on the images)

to an increase in thermal conductivity in the direction of the growth surface. At the same time, packing defects and plane defects accumulated in the film at the boundaries of the layers deposited during successive passes of the wire through the deposition zone. These defects were perpendicular to the direction of the heat flux through the substrate and, according to [27], reduced the thermal conductivity. However, the experiment in [27] found an increase in the thermal conductivity along the normal to the substrate with increasing film thickness suggested that the effect of the recrystallization factor dominated, reducing the grain boundary scattering of phonons.

Another factor that strongly influenced the temperature of the growth surface was the intensity of the light energy flux emitted by it. The emissivity of the surface, which is at the maximum for a black body, strongly increased with an increase in the roughness of the radiating surface [28, 29]. The roughness itself increased as the thickness of the HTS crystal layer increased. The overgrowth of $c_{\parallel}$-crystallites, rising above the average surface height, especially promoted an increase in roughness, an increase in emissivity, and a decrease in the temperature of the growth surface with constant heat supply from the heater.

An increase in the growth surface temperature by increasing the heater temperature, which seems to be the simplest solution counteracting the formation of $c_{\parallel}$-orientation is not an appropriate approach. In this approach, it was difficult to avoid the overheating of the underlying YBCO layers; the danger of their incongruent melting increased, since the deposition temperature was very close to the peritectic temperature. In addition, when the temperature rose above 1000 °C a noticeable degradation was observed in the substrate (oxidation of its reverse side, crystallization of the amorphous buffer Al_2O_3, the Y_2O_3 layers, causing additional roughness of the growth surface). Finally, the need for repeated adjustment of the heater temperature when applying successive YBCO layers significantly complicated the process of obtaining HTS wires.

An alternative method of preventing the growth of $c_{\parallel}$-crystallites is based on the creation of mechanical stresses in the growing YBCO film at the interface with the substrate or with an additionally introduced buffer layer. It was previously noted that on perovskite-like substrates with a minimum lattice mismatch with the *a*-parameter of YBCO, it was especially easy to switch $c_{\perp}$ growth to $c_{\parallel}$-growth (with a smaller film thickness and at a higher growth temperature) [30, 15]. On the contrary, films on substrates with a large parameter mismatch at the interface with YBCO, for example, on MgO, demonstrated a stable $c_{\perp}$ growth. These facts prompted some studies [13, 31], in which GdBCO/Gd_2O_3/$SrTiO_3$ and YBCO/$BaZrO_3$/MgO heterostructures, practically devoid of $c_{\parallel}$-crystallites due to buffer layers with a significant difference in parameters at the interface, were obtained.

In this study, we have applied the idea of introducing intermediate layers, causing stresses in the growing film and thus preventing the growth of $c_{\parallel}$-crystallites for the increase in the thickness of the HTS layer while maintaining the critical current density. Yttrium oxide was chosen for the intermediate layers for the following reasons: first, it can form epitaxial contacts with $YBa_2Cu_3O_{7-x}$, due to which, under high deposition temperatures, the chemical interaction typical of polycrystalline contacts of this system was absent [26]; second, the epitaxial nature of the contacts allowed preserving the sharp biaxial texture of the HTS layer, despite the introduction of a non-superconducting phase; third, Y_2O_3 is a simple oxide, therefore, during its precipitation, impairment of the cationic stoichiometry did not occur.

It is obvious that the development of parasitic $c_{\parallel}$-crystallites must be controlled during the stage of nucleation; however, during subsequent stages of growth it will be unproductive. Therefore, the deposition of YBCO and Y_2O_3 layers alternated starting from a thickness of ~ 100 nm. With the selected both movement speed of the substrate wire and the $Y(thd)_3$ precursor feeding rate, the thickness of deposited Y_2O_3 interlayers should have been ~ 10 nm. An XRD of the obtained composite samples with 4 interlayers of Y_2O_3 (Fig. 9a) showed a significant decrease in the number of $c_{\parallel}$-oriented crystallites in the films in comparison with YBCO films.

The same was evidenced by a comparison of the XRD data for films of YBCO and Y_2O_3

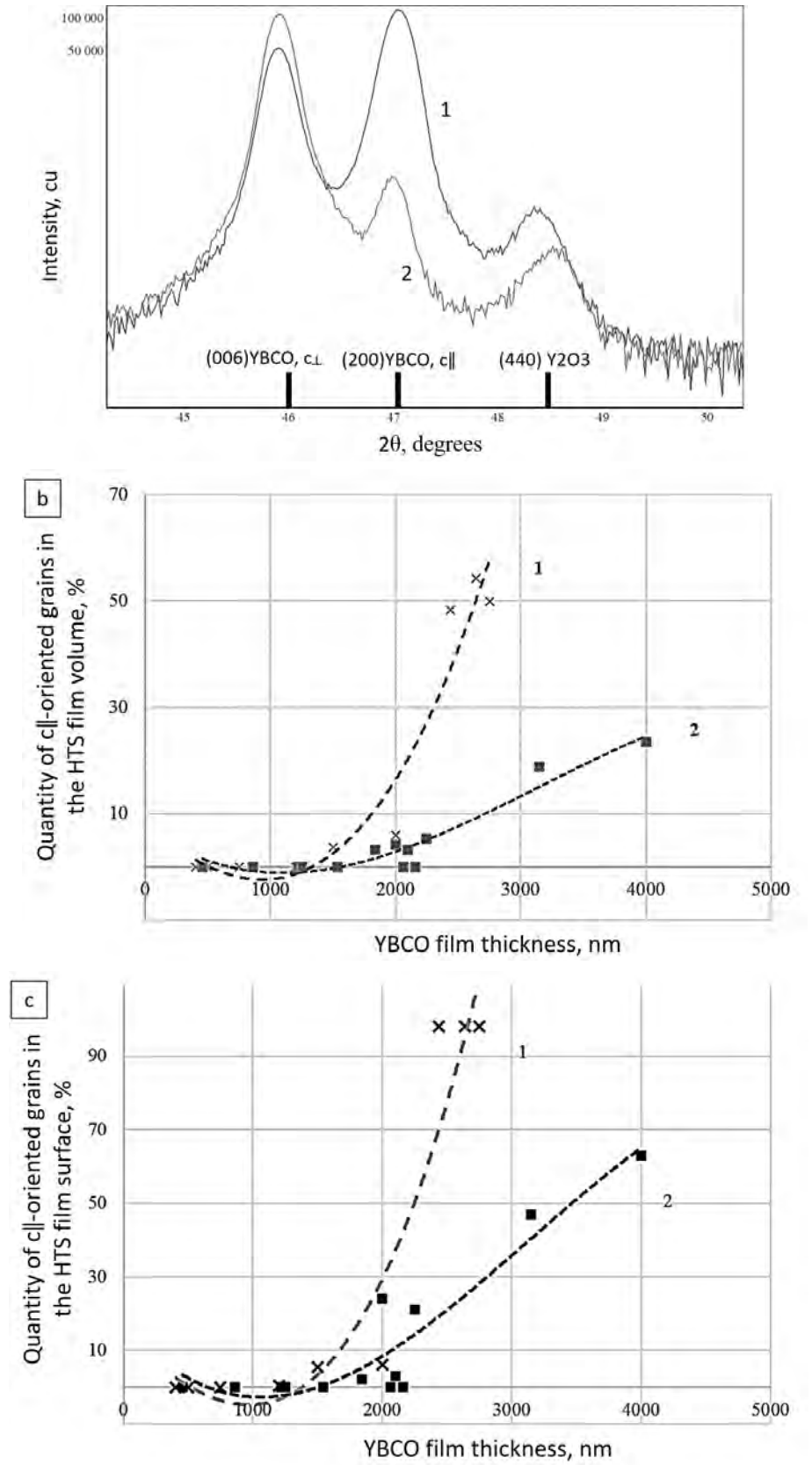

Fig. 9. The graphs of YBCO samples without interlayers (*1*) and with Y_2O_3 interlayers (*2*): XRD analysis of the samples with film thickness of 2000 nm (a); The comparison of $c_{\parallel}$-phase quantity on different film thicknesses: from XRD data (b), from SEM data (c)

composites obtained on a large set of samples in which the thickness of the HTS layers reached 4 μm (Fig. 9b): the introduction of Y_2O_3 interlayers can significantly reduce the proportion of $c_{\parallel}$-oriented crystallites in the film, and this effect was especially pronounced when the total thickness of the HTS layer exceeded 1500 nm. The alternation of YBCO and Y_2O_3 layers created an obstacle to YBCO growth in the $c_{\parallel}$-orientation, since the parameters of the crystal lattice of Y_2O_3 had a greater mismatch with it than the *c*-oriented YBCO film. The deposition of the upper layer of Y_2O_3 with different UC parameters creates an additional stress at the interface with the next YBCO layer, which causes a predominant growth of $c_{\perp}$-oriented crystallites, despite the obvious decrease in the surface temperature with a successive increase in the film thickness

For the control of the surface condition and understanding of the possibility of further deposition of HTS- layers with a high current density, all samples were studied by SEM with the measurement of the fraction of $c_{\parallel}$-crystallites on the surface (Fig. 9c) using the ImageJ software package. For all samples, the critical currents were also measured using the Superscan method. The results of these measurements are shown in Fig. 10 (a, b).

It was found that with a thickness close to 2 μm, with the absence of yttrium oxide interlayers, $c_{\parallel}$-oriented crystallites with a total film thickness of about 2400 nm occupied 98% of the surface, which was accompanied by the termination of the growth of the critical current with an increase in the film thickness. In films with interlayers the pattern changed significantly: the formation of Y_2O_3 layers noticeably decreased the density of $c_{\parallel}$-oriented crystallites; however, after a thickness of more than 2400 nm, the critical current in films with interlayers did not significantly increase (Fig.10a). Since, due to the presence of Y_2O_3 interlayers such films were thicker than similar films without interlayers, after recalculation for the critical current density, the differences in the current-carrying capacity of films with and without interlayers were not so large. The maximum j_c 2MA/cm^2 (77 K, SF) value was obtained for the composite film thickness of 1850 nm with six Y_2O_3 interlayers (Fig.10b).

The main reason for the decrease in j_c with a further increase in the thickness of the composite superconducting layer, was revealed using a TEM of cross sectioned samples. The morphology of a sample formed by successive deposition of ten YBCO layers with nine Y_2O_3 interlayers with a total thickness of the composite layer of 2.6 μm is shown in Fig. 11.

The photo clearly shows the darker YBCO layers and the lighter Y_2O_3 interlayers with a thickness close to 10 nm, located almost equidistantly, as was expected from the conditions of their deposition. Due to the colour contrast of matrix and interlayers $c_{\parallel}$-oriented YBCO crystallites can be distinguished easily: upon deposition the Y_2O_3 interlayer covered $c_{\parallel}$-crystallites protruding above the growth surfaces, thus rectangular steps were formed, some of which are shown in Fig. 11 with arrows. The TEM data of the cross section

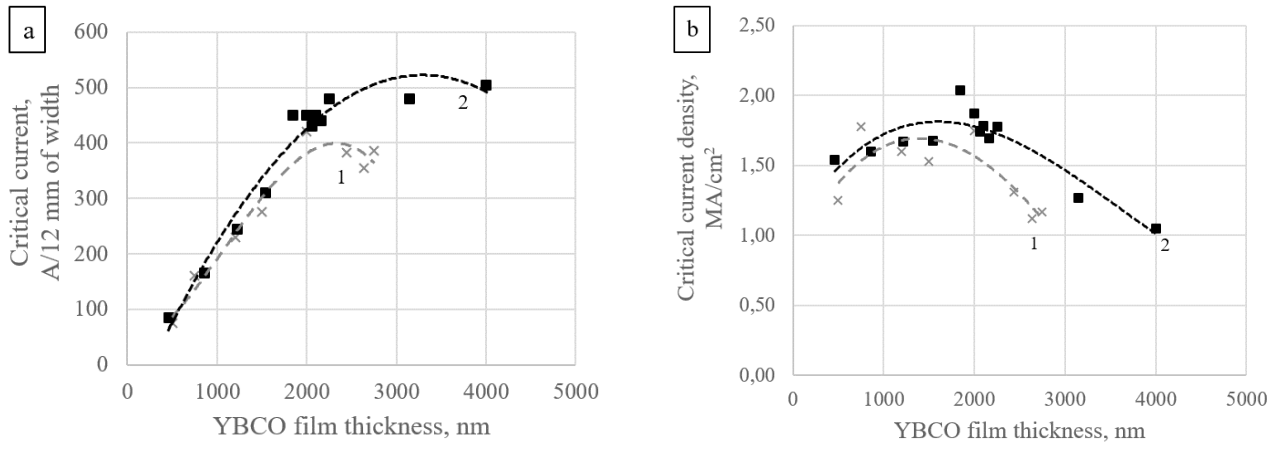

Fig. 10. The graphs of YBCO samples (*1*) and "YBCO + Y_2O_3 interlayers" composites (*2*): Thickness dependencies of: a) critical current (A/12 mm of width, 77 K, SF); b) critical current density (77 K, SF)

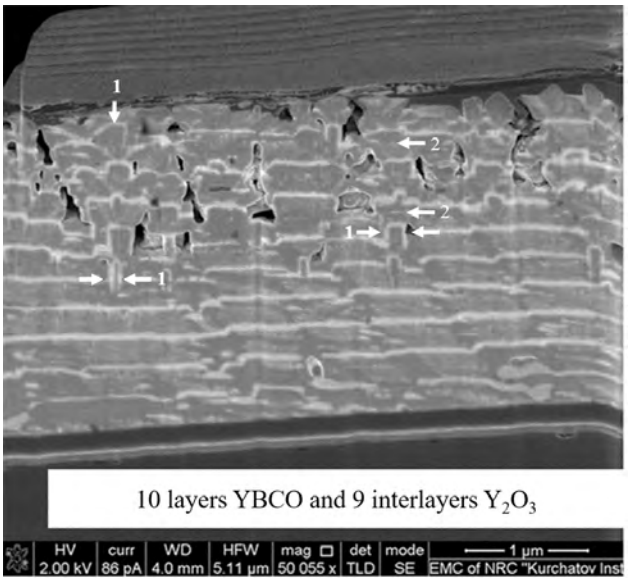

Fig. 11. SEM image of a cross-section of 10 layers of a YBCO sample with 9 Y_2O_3 interlayers: Y_2O_3 layer roughness caused by $c_{\parallel}$-crystallites (1); flat Y_2O_3 particles parallel to the substrate plane (2)

(Fig. 11) were consistent with the SEM results of the surface of films of different thicknesses (Fig. 9c). Indeed, both methods revealed the formation of $c_{\parallel}$-crystallites in composite films in a noticeable concentration, starting with a thickness of ~ 1 µm.

The good conformity of the interlayers (Y_2O_3 layers with the uniform thickness covered faces of $c_{\parallel}$ and $c_{\perp}$-crystallites), which was a consequence of the epitaxial nature of these contacts and low surface tension at the interface. The TEM results in Figs. 11 and 12 revealed an important feature of the morphology of composites, which confirmed the initial hypothesis of this study: Y_2O_3 interlayers completely cover $c_{\parallel}$-oriented grains and block their further growth along the plane *ab*, during the deposition of the next YBCO layer on the Y_2O_3 only $c_{\perp}$-oriented crystallites are nucleated. This was confirmed by Figs. 11 and 12, the orientation of the YBCO layers adjacent to $c_{\parallel}$-crystallite is shown on Fig. 12 by arrows indicating the crystallographic axes.

In the YBCO matrix, multiple inclusions of Y_2O_3 nanoparticles predominantly in the form of flat flakes elongated along the plane of the substrate were clearly visible. These particles were formed as a result of the deliberately enriched composition of YBCO with the yttrium component in comparison with the stoichiometry of 1:2:3 [16]; they must play the role of pinning centres increasing the stability of the critical current of a superconductor in a magnetic field.

Starting from a thickness of ~ 1.5 µm, nanosized pores started to form in the composite layer. They are clearly visible in Fig. 11 and enlarged in Fig. 12b. This phenomenon was noted in [11], but there is still no clear understanding of the reasons for their formation. The TEM results allowed proposing the following scenario for the formation of nanopores. For the gas phase epitaxial crystallization of films of multicomponent phases, in particular, $YBa_2Cu_3O_{6.5}$ it is necessary that each of the components in the vapour reach the growth surface and be able to freely move along it due to the surface diffusion of atoms or ions.

Colonization of the growth surface with $c_{\parallel}$-oriented crystallites noticeably changes both the accessibility of this surface for particles in vapour and the conditions of surface diffusion. Between the walls of adjacent $c_{\parallel}$-crystallites "wells" with an aspect ratio of $\geqslant 2$ formed (Fig. 12b), the conformal filling of which with a $c_{\perp}$ YBCO layer becomes difficult. It is known from the fundamentals of gas dynamics and mass transfer that a diffusion layer forms above the film growth surface. This barrier must be overcome by particles from the gas phase in order to reach the surface. The thickness of this layer increases at the lowering of the gas flow rate and it is obvious that in "wells", where the flow rate is low, the diffusion layer has the greatest thickness and provides the greatest resistance to the penetration of YBCO components into the growth surface. It should be noted that the inner surface of nanopores in the composites obtained by us was conformally coated with a Y_2O_3, and in the study [13], dense filling of spaces between neighbouring $c_{\parallel}$-crystallites of YBCO with copper oxide was noted on TEM-images, i.e., the delivery of the yttrium and copper components from the vapour completely ensures the filling of nanopores. It can be argued with great certainty that the lack of the barium component prevents the formation of the HTS phase between neighbouring $c_{\parallel}$-crystallites, which can be attributed to the high molecular weight of the particles supplying the barium component, although their true composition is unknown.

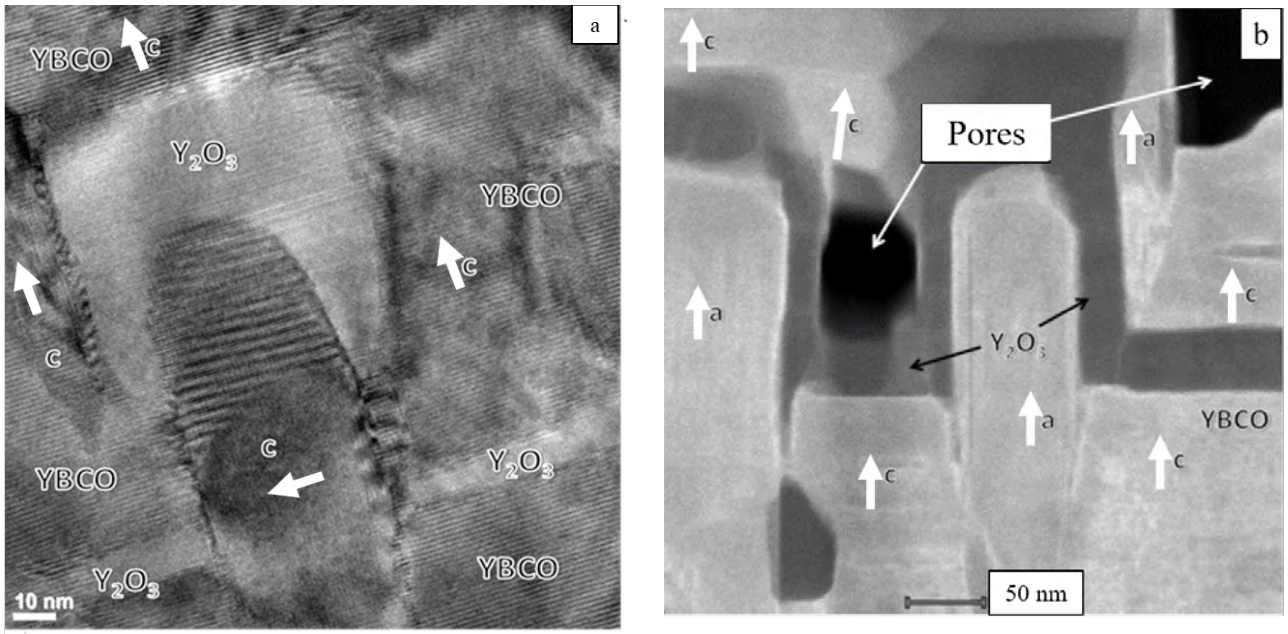

Fig. 12. TEM images of the areas with $c_{\parallel}$-oriented crystallites covered by Y_2O_3 layer: $c_{\perp}$-oriented YBCO growth on $c_{\parallel}$-oriented crystallite is demonstrated (a); Pore formation near $c_{\parallel}$ oriented crystallites (b)

$c_{\parallel}$-crystallites rising above the surface significantly increased the roughness of the surface. This contributes to its cooling and sharply increases the path of surface diffusion which the adsorbed particles of the components must pass before they will occupy places with a local minimum of energy. As a result, the surface diffusion flux turned out to be insufficient for providing the conformal growth of the phase, primarily in the spaces between closely-spaced vertical $c_{\parallel}$-crystallites. Comparing the values of the atomic masses and radii of the cations composing the $YBa_2Cu_3O_{6.5}$ phase, it can be argued that the least diffusion-mobile was the largest and "heaviest" cation, Ba^{2+}, therefore, the local deficiency of barium (arising from the difficulties of its delivery through the surface diffusion layer) cannot be compensated for by its lateral diffusion movement. Thus, it can be argued that superficial $c_{\parallel}$-crystallites complicated both successive stages of gas phase epitaxy of YBCO, which are the supply of nutrients to the growth surface and surface diffusion along it. As a result of the close location of neighbouring $c_{\parallel}$ crystallites between them, places not filled with the crystallizing YBCO phase arose, i.e., nanopores lowering the critical current density of superconducting layers of large thickness.

Conclusions

Heteroepitaxial layers of a high-temperature YBCO superconductor and laminated composites $YBCO/Y_2O_3$, components of 2G HTS wires, were obtained in deposition mode on a continuously moving wire substrate by the MOCVD method. It was shown that after reaching the YBCO thickness of ~ 1900 nm, the preferred orientation of the growth of the $YBa_2Cu_3O_{7-x}$ phase in the surface layer changes, as a result of which the surface is covered with $c_{\parallel}$-crystallites preventing the passage of the superconducting current in the direction along the substrate wire; this circumstance lowers the critical current density and does not allow an increase in the current-carrying capacity by increasing the thickness of the HTS layer. It was shown that the method of scanning electron microscopy is more informative than the XRD for the analysis of the orientation of surface crystallites. The method for reducing the concentration $c_{\parallel}$-oriented crystallites in laminated $YBCO/Y_2O_3$ composites was proposed and experimentally tested. It was shown that thin (~ 10 nm) layers of Y_2O_3 prevent the emergence and development of $c_{\parallel}$-oriented crystallites, they do not impair the highly oriented state of the HTS matrix, and they allow obtaining predominantly $c_{\perp}$-oriented YBCO layers with a thickness up to 4 μm. Due to this, it was possible

to increase the critical current by 25–30% and obtain wires with a current-carrying capacity of 500 A (12 mm wide, 77 K, in the intrinsic magnetic field), while maintaining a high critical current density (j_c > 2 MA/cm). Using the TEM method, it was shown that the main reason for the decrease in j_c with a further increase in the thickness of the composites is the formation of nanopores in the near-surface layer of the growing film. The reasons for the appearance of nanopores were analysed and it was concluded that they were formed due to the proximity of $c_{\parallel}$-oriented crystallites, causing an increase in the thickness of the diffusion near-surface boundary layer and inhibiting the surface diffusion flow. It was suggested that during the formation of nanopores, the difficulties with delivery to the surface from the vapour and difficulties in surface diffusion were characteristic primarily for the barium component of the HTS.

Conflict of interests

The authors declare that they have no known competing financial interests or personal relationships that could have influenced the work reported in this paper.

References

1. Fleshler S., Buczek D., Carter B., Ogata M. Scale-up of 2G wire manufacturing at American Superconductor Corporation. *Physica C*. 2009;469(15-20): 1316–1321. https://doi.org/10.1016/j.physc.2009.05.234

2. Nagaishi T., Shingai Y., Konishi M., Taneda T., Ota H., Honda G., Kato T., Ohmatsu K. Development of REBCO coated conductors on textured metallic substrates. *Physica C*. 2009;469(15-20): 1311–1315. https://doi.org/10.1016/j.physc.2009.05.253

3. Rosner C. H. Superconductivity: star technology for the 21st century. *IEEE Transactions on Applied Superconductivity*. 2001;11(1): 39–48. https://doi.org/10.1109/77.919283

4. Mansour R. R. Microwave superconductivity. *IEEE Transactions on Microwave Theory and Techniques*. 2002;50(3): 750–759. https://doi.org/10.1109/22.989959

5. Hayakawa H., Yoshikawa N., Yorozu S., Fujimaki A. Superconducting digital electronics. *Proceedings of the IEEE*. 2004;92(10): 1549–1563. https://doi.org/10.1109/JPROC.2004.833658

6. Wimbush S. C. Large scale applications of HTS in New Zealand. *Physics Procedia*. 2015;65: 221–224. https://doi.org/10.1016/j.phpro.2015.05.125

7. Zhu J., Zheng X., Qiu M., Zhang Z., Li J., Yuan W. Application simulation of a resistive type superconducting fault current limiter (SFCL) in a transmission and wind power system. *Energy Procedia*. 2015;75: 716–721. https://doi.org/10.1016/j.egypro.2015.07.498

8. Iwasaki H., Inaba S., Sugioka K., Nozaki Y., Kobayashi N. Superconducting anisotropy in the Y-based system substituted for the Y, Ba and Cu sites. *Physica C*. 1997;290: 113. https://doi.org/10.1016/S0921-4534(97)00634-5

9. Freyhardt H. C., Hellstrom E. E. High-temperature superconductors: A Review of $YBa_2Cu_3O_{6+x}$ and $(Bi,Pb)_2Sr_2Ca_2Cu_3O_{10}$. *Cryogenic Engineering*. New York: Springer; 2007. pp. 309–339. https://doi.org/10.1007/0-387-46896-X

10. Dimos D., Chaudhari P., Mannhart J. Superconducting transport properties of grain boundaries in $YBa_2Cu_3O_7$ bicrystals. *Phys. Rev. B*. 1990;41: 4038–4049. http://dx.doi.org/10.1103/PhysRevB.41.4038

11. Goyal A. (ed.) *Second-Generation HTS Conductors*. Boston/Dordrecht/New York/London: Kluwer Academic Publ.; 2009. 432 p.

12. Zhang H., Yang J., Wang S., Wu Y., Lv Q., Li S. Film thickness dependence of microstructure and superconductive property of PLD prepared YBCO layers. *Physica C*. 2014;499: 54–56. https://doi.org/10.1016/j.physc.2014.01.001

13. Markelov A. V., Samoilenkov S. V., Akbashev A. R., Vasiliev A. L., Kaul A. R. Control of orientation of $RBa_2Cu_3O_7$ films on substrates with low lattice mismatch via seed layer formation. *IEEE Transactions on Applied Superconductivity*. 2011;21(3): 3066–3069. https://doi.org/10.1109/TASC.2010.2102992

14. Granozio F. M., Salluzzo M., Scotti di Uccio U., Maggio-Aprile I., Fischer O. Competition between a-axis and c-axis growth in superconducting $RBa_2Cu_3O_{7-x}$ thin films. *Phys. Rev. B*. 2000;61(1): 756–765. https://doi.org/10.1103/PhysRevB.61.756

15. Jeschke R. Schneider G. Ulmer G. Linker influence of the substrate material on the growth direction of YBaCuO thin films. *Physica C*. 1995;243: 243–251. https://doi.org/10.1016/0921-4534(95)00019-4

16. Moyzykh M., Boytsova O., Amelichev V, Samoilenkov S., Voloshin I., Kaul A., Lacroix B., Paumier F., Gaboriaud R. Effects of yttrium oxide inclusions on the orientation and superconducting properties of YBCO films. *Kondensirovannye sredy i mezhfaznye granitsy = Condensed Matter and Interphases*. 2013;15(2): 91-98. Available at: http://www.kcmf.vsu.ru/resources/t_15_2_2013_001.pdf

17. *2G HTS Wire Specification Overview*. Available at: http://www.superpower-inc.com/system/files/

SP_2G+Wire+Spec+Sheet_2014_web_v1_0.pdf (accessed 29 October 2016).

18. Murakami M., Gotoh S., Fujimoto H., Yamaguchi K., Koshizuka N., Tanaka S. Flux pinning and critical currents in melt processed YBaCuO superconductors. *Superconductor Science and Technology*. 1991;4: S43–S50. https://doi.org/10.1088/0953-2048/4/1S/005

19. Zhao P., Ito A., Goto T. Rapid deposition of YBCO films by laser CVD and effect of lattice mismatch on their epitaxial growth and critical temperature. *Ceramics International*. 2013;39: 7491–7497. https://doi.org/10.1016/j.ceramint.2013.02.098

20. Zhao P., Ito A., Goto T., Tu R. High-speed growth of $YBa_2Cu_3O_{7-\delta}$ film with high critical temperature on MgO single crystal substrate by laser chemical vapor deposition. *Superconductor Science and Technology*. 2010;23(12): 125010. https://doi.org/10.1088/0953-2048/23/12/125010

21. Zhao P., Ito A., Goto T., Tu R. Fast epitaxial growth of *a*-axis- and *c*-axis-oriented $YBa_2Cu_3O_{7-\delta}$ films on (1 0 0) $LaAlO_3$ substrate by laser chemical vapor deposition. *Applied Surface Science*. 2010;257: 4317–4320. https://doi.org/10.1016/j.apsusc.2010.12.047

22. Hammond R. H., Bormann R. Correlation between the in situ growth conditions of YBCO thin films and the thermodynamic stability criteria. *Physica C*. 1989;162-164: 703–704. https://doi.org/10.1016/0921-4534(89)91218-5

23. Voronin G. F., Degterov S. A. Solid State Equilibria in the Ba-Cu-O System. *J. Solid State Chem*. 1994;110(1): 50–57. (and references therein). https://doi.org/10.1006/jssc.1994.1134

24. Lindemer T. B., Specht E. D. The BaO-Cu-CuO system. Solid-liquid equilibria and thermodynamics of $BaCuO_2$ and $BaCu_2O_2$. *Physica C*. 1995;255(1-2): 81–94. (and references therein). https://doi.org/10.1016/0921-4534(95)00460-2

25. Samoylenkov S. V., Gorbenko O. Yu, Graboy I. E., Kaul A. R., Zandbergen H. W., Connolly E. Secondary phases in (001)$RBa_2Cu_3O_{7-\delta}$ epitaxial thin films. *Chemistry of Materials*. 1999:11(9): 2417–2428. https://doi.org/10.1021/cm991016v

26. Kaul A. R., Gorbenko O. Yu., Kamenev A. A. The role of heteroepitaxy in the development of new thin-film oxide-based functional materials. *Russian Chemical Reviews*. 2004;73(9): 932–953. https://doi.org/10.1070/RC2004v073n09ABEH000919

27. Murakami Y., Goto H., Taguchi Y., Nagasaka Y. Measurement of out-of-plane thermal conductivity of epitaxial $YBa_2Cu_3O_{7-\delta}$ thin films in the temperature range from 10 K to 300 K by photothermal reflectance. *International Journal of Thermophysics*. 2017;38(10): 160. https://doi.org/10.1007/s10765-017-2294-7

28. Agababov S. G., Vliyanie sherohovatosti poverhnosti tverdogo tela na ego radiatsionnie svoistva I metody ih eksperimentalnogo opredeleniya [Influence of the surface roughness of a solid on its radiation properties and methods of their experimental determination]. *Teplofizika visokih temperatur*. 1968;6(1): 78–88. (In Russ.)

29. Sayapina V. I., Svet D. Ya., Popova O. R., Vliyanie sherohovatosti poverhnosti na izluchatelnuyu sposobnost metallov [Influence of surface roughness on the emissivity of metals]. *Teplofizika visokih temperatur*. 1972;10(3): 528–535. (In Russ.)

30. Mukaida M., Miyazawa S. Nature of preferred orientation of $YBa_2Cu_3O_x$ thin films. *Japanese Journal of Applied Physics*. 1993;32(10): 4521–4528. https://doi.org/10.1143/jjap.32.4521

31. Markelov A. V. *The influence of buffer layers on the oriented growth of $RBa_2Cu_3O_{7-\delta}$ (R – rare earth element) films and their superconducting characteristics*. Thesis of Cand. in Chem. Moscow: MSU (Lomonosov University); 2011. 108 p.

Information about the authors

Alexander E. Shchukin, PhD student, Chemistry Department, Lomonosov Moscow State University, Moscow, Russian Federation; e-mail: aleksandr.shukin@mail.ru. ORCID iD: https://orcid.org/0000-0002-3502-2950.

Andrey R. Kaul, DSc in Chemistry, Professor, Chemistry Department, Lomonosov Moscow State University, Moscow, Russian Federation; e-mail: arkaul@mail.ru. ORCID iD: https://orcid.org/0000-0002-3582-3467.

Alexander L. Vasiliev, PhD in Physics and Mathematics, Associate Professor, Leading Researcher of the Resource Center for Probe and Electron Microscopy of the National Research Center "Kurchatov Institute", Head of the Laboratory of Electron Microscopy of Federal Research Center "Crystallography and photonics" of the Shubnikov Institute of Crystallography of Russian Academy of Science, Moscow, Russian Federation; e-mail: a.vasiliev56@gmail.com. ORCID iD: https://orcid.org/0000-0001-7884-4180.

Igor A. Rudnev, DSc in Physics and Mathematics, Professor, Institute of Laser and Plasma Technologies, National Research Nuclear University "Moscow Engineering Physics Institute", Moscow, Russian Federation; e-mail: iarudnev@mephi.ru. ORCID iD: https://orcid.org/0000-0002-5438-2548.

All authors have read and approved the final manuscript.

Received 2 January 2021; Approved after reviewing 15 February 2021; Accepted 15 March 2021; Published online 25 March 2021

Translated by Valentina Mittova
Edited and proofread by Simon Cox